Journal of Chromatography A, 1218 (2011) 5520–5526

Contents lists available at ScienceDirect

Journal of Chromatography A

journal homepage: www.elsevier.com/locate/chroma

Size separation of colloidally dispersed nanoparticles using a monolithic capillary column

Kumiko Sakai-Kato[a,*], Shigenori Ota[b], Toyohide Takeuchi[c], Toru Kawanishi[a]

[a] Division of Drugs, National Institute of Health Sciences, 1-18-1 Kamiyoga, Setagaya-ku, Tokyo 158-8501, Japan
[b] R & D Department, GL Sciences Inc. 237-2 Sayamagahara, Iruma, Saitama 358-0032, Japan
[c] Department of Chemistry, Faculty of Engineering, Gifu University, 1-1 Yanagido, Gifu 501-1193, Japan

ARTICLE INFO

Article history:
Received 12 November 2010
Received in revised form 14 June 2011
Accepted 14 June 2011
Available online 22 June 2011

Keywords:
Nanoparticles
Monolithic column
Size exclusion chromatography

ABSTRACT

We developed a method to separate colloidally dispersed nanoparticles on monolithic capillary columns. Silica nanoparticles were eluted according to their sizes, and the plots of the logarithm of the size of nanoparticles against their elution volume showed good linearity ($r = 0.992$) over wide range of sizes. Because of the high porosity of the monolithic column (porosity; 88%), the column's length could be increased without clogging of the dispersed samples and the pressure in a long column (500 mm × 0.2 mm i.d.) was low, with a value of 5.8 MPa at a flow rate of 1 μL/min. We demonstrate that this method using monolithic capillary columns could be used as a powerful tool for size separation of nanometer-size materials, which will open a new pathway to quality control of nanomaterials in nanotechnology applications.

1. Introduction

Recent advances in nanotechnology have enabled the development of modern drug carrier systems that play an important role in the controlled delivery of pharmacological agents to their targets at a therapeutically optimal rate and dose [1]. "Soft" nanocarriers including micelles, polymers, and lipid nanoparticles have been used for drug delivery [2,3]. Carriers with greater hardness or density, including colloidally dispersed nanoparticles composed of silica, gold, or iron oxide, also have been used for drug and gene therapeutics and for diagnostic imaging [4,5]. These colloidally dispersed nanoparticles are also important in other fields: for example, gold nanoparticles have been used as imaging tools [6]; titanium dioxide particles have been used as self-cleaning, anti-bacterial agents and UV protecting agents [7,8]; and cadmium selenide has been used to create semiconductor nanocrystals (quantum dots) [9].

Exact knowledge of the size and size distribution of these nanoparticles is essential for their application in nanoparticulate drug delivery systems, because the nanoparticles' size can substantially affect their physicochemical and biopharmaceutical behavior. For example, variations in particle size can change drug release kinetics or transport phenomena across biological barriers, as well as pharmacokinetics in the human body [10–12].

Fractionation techniques offer advantages over non-fractionation techniques for particle sizing because fractionation techniques produce information about average particle size and the distribution of particle sizes for a given sample. Non-fractionation techniques, such as photon correlation spectroscopy, suffer from lower resolution than that afforded by fractionation techniques and thus are not as well suited for the analysis of samples with broad particle size distributions.

Among methods for the size analysis and characterization of macromolecules, flow-assisted techniques such as size exclusion chromatography (SEC) [13,14], hydrodynamic chromatography (HDC) [15,16], field-flow fractionation (FFF) [17–19] and capillary hydrodynamic fractionation [20] are suitable for separation of samples on the basis of differences in the physical size indexes of the analytes.

When colloids possess an electric charge in buffered aqueous solutions, electrophoretic separation methods are also among those utilized methods for particle separation and characterization. Reports have been made to employ capillary electrophoresis for analytical separations of charged particulate materials, mostly carried out by capillary zone electrophoresis [21–23].

SEC is the most commonly used fractionation method for particle sizing. Usually, SEC is performed on a column packed with polymer gel or porous silica microparticles with pore-size distributions over the range of a few to a few hundred nanometers. Polymer samples are separated with such packed SEC columns [13]. In addition, nanoparticulate drug carriers such as liposomes are often separated from small solutes by means of SEC [24].

* Corresponding author. Tel.: +81 3 3700 9662; fax: +81 3 3700 9662.
E-mail address: kumikato@nihs.go.jp (K. Sakai-Kato).

0021-9673/$ – see front matter © 2011 Elsevier B.V. All rights reserved.
doi:10.1016/j.chroma.2011.06.055

Recently, Ute et al. reported SEC of a polystyrene polymer on monolithic silica columns using tetrahydrofuran (THF) as the eluent [25]. Monolithic silica columns have received much attention as a newly introduced technology for HPLC and capillary electrochromatography [26]. These columns consist of a single piece of porous material (most often polymer- or silica-based) with a bimodal pore structure consisting of "throughpores" (pore size ~1.5–5 μm) and "mesopores in the skeleton" (~10–25 nm) [27]. Typically, monolithic columns provide higher porosity compared to conventional columns packed with spherical particles, and such higher porosity results in much lower column backpressure. Furthermore, the throughpore/skeleton size ratio of 2–4 in a monolithic column is much greater than the ratio of 0.25–0.4 typically found in a column packed with particles [28]. This increased size ratio enables the use of a long column, thus leading to high separation efficiency [29]. The sizes of the skeletons and throughpores can be independently controlled by changing the preparation conditions, including the nature of the porogen.

In this paper, we report the size separation of colloidally dispersed nanoparticles by means of a monolithic capillary column. We used monolithic columns consisting of silica derivatized with an amide group, i.e., a neutral hydrophilic bond that prohibits the adsorption of samples on the silica monolith by ion-exchange interaction and that would enable the analysis of charged soft nanocarriers such as liposomes derived from biomaterials. We analyzed the colloidal silica nanoparticles by their sizes using a monolithic capillary column. We expected that the high porosity of the monolithic columns would prevent colloidal samples from clogging the columns.

2. Materials and methods

2.1. Chemicals

Silica nanoparticles (Cataloid S) with sizes of 5, 11, 26, 45, and 78 nm were obtained from JGC Catalysts and Chemicals Ltd. (Kanagawa, Japan). Methanol (HPLC grade) and dextran standards were obtained from Sigma–Aldrich Corporation (St. Louis, MO, USA). Sodium nitrate was from Kanto Chemicals (Tokyo, Japan). Samples were dissolved or dispersed in eluent and filtered through a 0.20-μm filter (Millex-LG, Millipore Corp., Tokyo, Japan) prior to being applied to the columns. Polydiversity index (PDI) of silica nanoparticles and hydrodynamic diameters of dextran standards in eluent were measured using dynamic light scattering measurement (ZetasizerNano, Malvern, UK).

2.2. LC conditions

Sample separation was performed with a capillary LC system equipped with a capillary HPLC pump (MP711V; GL Sciences, Tokyo, Japan), a four-port internal sample injector (fixed volume: 10 nL; Valco Instrument Co. Inc., Houston, TX, USA), and a capillary ultraviolet–visible (UV–Vis) detector (MU701; GL Sciences).

Samples were analyzed on a MonoCap Amide column (500 mm × 0.2 mm; 1 μm skeleton, 2 μm throughpore, and 15 nm mesopore; GL Sciences). The permeability is represented by a K value ($K = u\varepsilon_0\eta L/\Delta P$, where u stands for the linear velocity of the eluent, ε_0 for total porosity of the column, η for solvent viscosity, L for column length, and ΔP for pressure drop [30]). Permeability was measured in 10 mM sodium phosphate buffer (pH 7.2) containing methanol (20% v/v). The total porosity of the column, ε_0 was estimated using void times of hollow capillary column and monolithic capillary column, and total volume of the column. The mobile phase consisted of a 10 mM sodium phosphate buffer (pH 7.2) containing methanol (20% v/v). The mobile phase was delivered at a rate of 0.1–1 μL/min and the column was kept at room temperature. The detector was operated at a wavelength of 210 nm. A sample volume of 10 nL was injected for each analysis. The morphology of the monolithic silica was examined by a scanning electron microscope (SEM; S-3000N, Hitachi). For the measurement of flow rate, we used a flowmeter composed of 5-μL microsyringe attached to the end of the column.

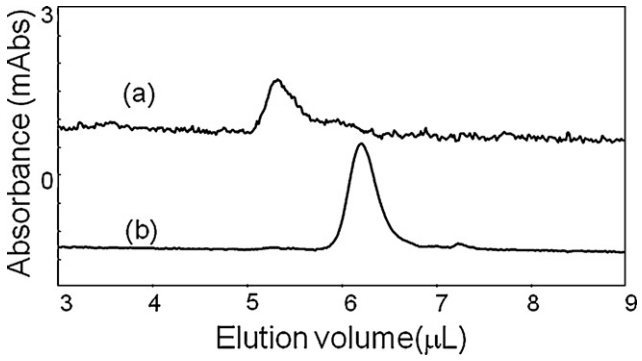

Fig. 1. Effect of eluent composition on elution profile of a sample of 26 nm silica nanoparticles. Column: Capillary EX nano Monocap Amide (250 mm × 0.2 mm i.d.); eluent: (a) water or (b) 10 mM phosphate buffer (pH 7.2); flow rate: 1 μL/min.

3. Results and discussion

Usually, SEC is performed with a column packed with polymer gel or porous silica microparticles. However, such columns could become clogged when used to separate colloidally dispersed nanoparticles with sufficient hardness or high density, such as inorganic nanoparticles. Therefore, in this study monolithic capillary columns with high porosity were used for the analysis of colloidally dispersed nanoparticles.

3.1. Detection

In this study, we used different sizes of silica nanoparticles. The detection method used was based on turbidimetric detection, in which colloidal species are observed with a UV–Vis detector [31,32]. Although silica nanoparticles do not contain any chromophores, it is expected that a portion of incident UV light is scattered by the silica nanoparticles, thereby reducing the intensity of light reaching the photomultiplier. This reduction in light intensity provides an apparent absorption value. In this experiment, we used different concentrations of silica nanoparticles depending on their sizes, because the larger the silica colloid, the larger the pseudo-UV absorbance observed. To achieve an optimal signal-to-noise ratio, the detector wavelength was set to 210 nm for the experiments described here.

3.2. Optimization of eluent

It is important that the silica nanoparticles maintain a consistent size during analysis; therefore, an eluent should be chosen that does not cause gelation, aggregation, or dissolution of the particles. As shown by the unstable baseline and small sample peak in Fig. 1(a), water was not appropriate as an eluent compared with phosphate buffer (Fig. 1(b)). It is considered that the silica nanoparticles probably are not stable and coagulated in plain water, and silica nanoparticles are prone to clogging injectors or columns which lead to small peak area in plain water [33]. For these reasons we used phosphate buffer as the eluent in our studies.

We also examined the effect of the eluent pH on the peak area and plate number of silica nanoparticles. We used 10 mM phos-

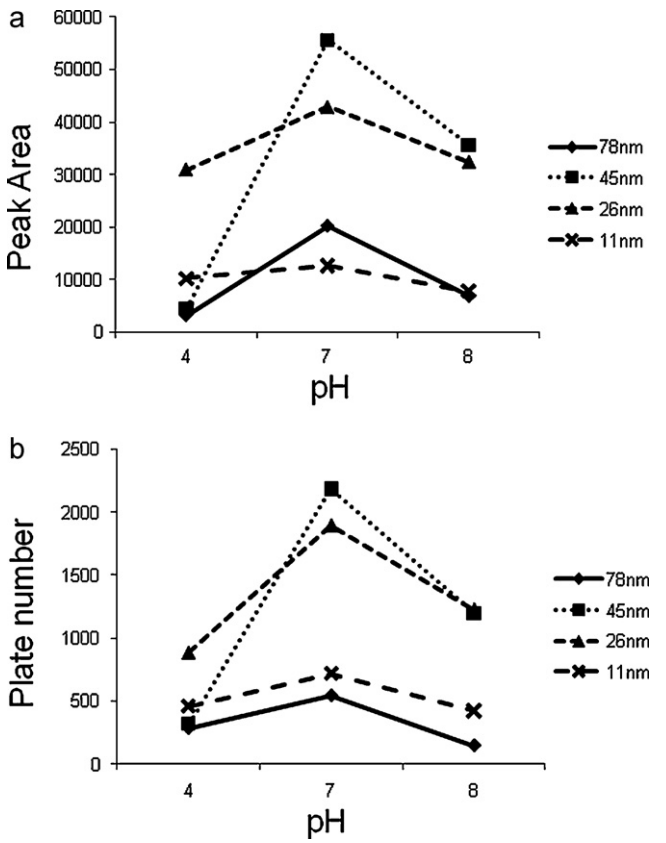

Fig. 2. Effect of eluent pH on (a) peak area and (b) plate number of various sizes of silica nanoparticles. Eluent: 10 mM phosphate buffer (pH 4, 7.2, or 8); sample: 0.3% (w/v) 78 nm, 0.5% (w/v) 45 nm, 1% (w/v) 26 nm, and 1% (w/v) 11 nm silica nanoparticles. Each sample containing one size of particles. Other conditions are the same as those described in Fig. 1.

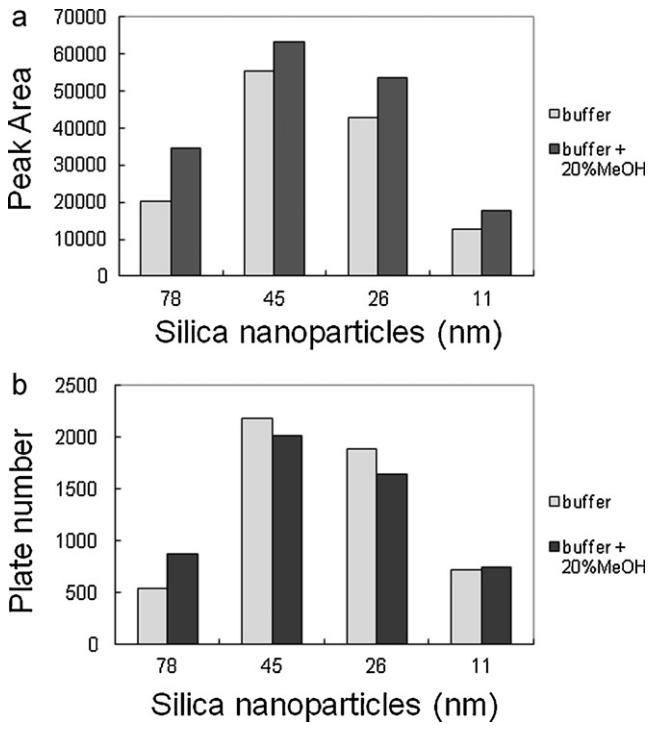

Fig. 3. Effect of methanol ratio in the eluent on (a) peak area and (b) plate number of various sizes of silica nanoparticles. Eluent: 10 mM phosphate buffer (pH 7.2) or 10 mM phosphate buffer (pH 7.2) containing 20% methanol. The other chromatographic conditions were the same as in Fig. 2.

phate buffer at pH 4, 7.2, and 8. As shown in Fig. 2, both the peak area and the plate number were the largest at pH 7.2 for all sizes of silica nanoparticles. It is probable that coagulation of silica nanoparticles takes place at lower pH, due to a decrease in electrostatic repulsion, and silica nanoparticles are prone to clogging injectors or columns which lead to small peak area in plain water. Considering the above results and the stability of the separation column, we used phosphate buffer at pH 7.2 in our studies.

Examining the effect of phosphate buffer concentration on sample peak size, we found that the sample peak area was larger in 10 mM phosphate buffer than it was in 50 mM phosphate buffer. This difference was most pronounced for the sample of 78-nm silica nanoparticles (data not shown). The decrease in peak area with increasing buffer concentration was probably caused by nanoparticle coagulation that would have been induced by high concentrations of sodium cations in the buffer [34]. Therefore, we used 10 mM phosphate buffer (pH 7.2) in our experiments.

Finally, we examined the effect of organic solvent on sample peak area. Because slightly larger peak areas were observed with methanol than with acetonitrile, we selected methanol as an organic solvent (data not shown). This preference for methanol may be ascribed to a different hydrogen bonding force between silica nanoparticles and methanol or acetonitrile. By adding methanol at 20% (v/v) to the eluent, peak areas of all sample peaks were increased; however, the plate number did not increase for all sizes of nanoparticles (Fig. 3). Further increases in the organic solvent ratio up to 90% (v/v) largely decreased the peak area. This observed decrease in peak area with increasing organic solvent ratio probably occurred because the presence of the solvent decreased the electric double layer around the nanoparticles, which would have resulted in the reduction of repulsion between each nanoparticle and thus increased particle aggregation. Therefore, 20% methanol was added to the phosphate buffer in our experiments. When 10 mM phosphate buffer (pH 7.2) containing 20% methanol was used as the eluent, the pressure in a long column (500 mm × 0.2 mm i.d.) was low, with a value of 5.8 MPa at a flow rate of 1 μL/min. Under this condition, the permeability K was 6.7×10^{-14} m^2 and the total porosity of the column was 88%.

3.3. *Effect of column length and flow rate on silica nanoparticle separation*

The use of longer monolithic columns would be one possible way to better separate mix samples. Fig. 4(a) shows the effect of column length on column efficiency for silica nanoparticles with different sizes. We used 150, 250, and 500 mm columns; these are all that are commercially available. The column efficiency slightly increased with column length for all silicate nanoparticles using the same eluent and flow rate (1 μL/min). This result is probably explained by the external-band broadening contributions [35]. The contribution of external-band broadening contributions to total system efficiency was larger as the column length decreased and the ratio of extra-column variance to total system variance were 37, 54, 78%, when nanoparticles of size of 78 nm were analyzed onto 500, 250, and 150 mm columns, respectively. The extra-column variance was calculated by measuring the half bandwidth of nanoparticle peak analyzed without column. Although using a longer column takes a longer time to elute solutes, it has an advantage for better separation of a mixture sample, In fact, as shown in Fig. 4(b), the separation of silica nanoparticles mixture was gradually improved by using longer column length, although the elution time is getting longer.

Further, we examined the effect of flow rate on column efficiency to improve the separation of the silica nanoparticle mixture. We confirmed the accuracy and precision of flow rate with various

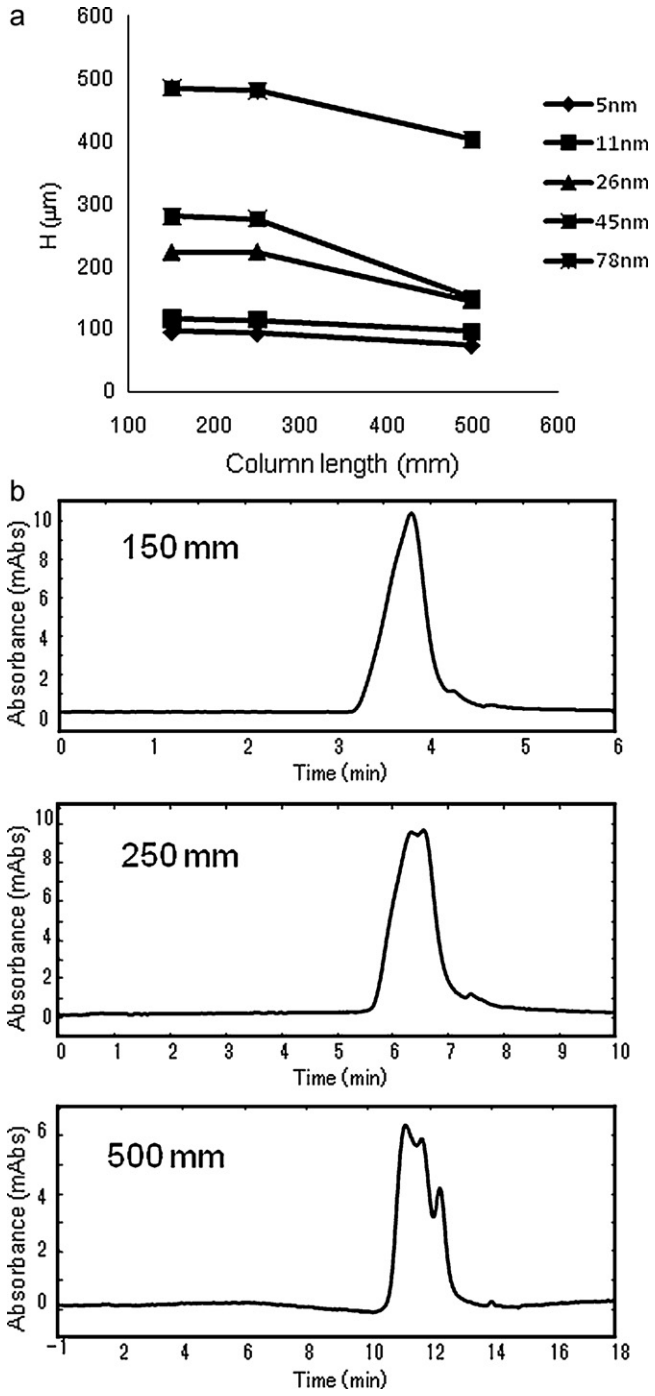

Fig. 4. Effect of column length on (a) plate number and (b) silica nanoparticle separation. Column: Capillary EX nano Monocap Amide (150, 250, and 500 mm × 0.2 mm i.d.); eluent: 10 mM phosphate buffer (pH 7.2) containing 20% methanol; sample: (a) 0.3% (w/v) 78 nm, 0.5% (w/v) 45 nm, 1% (w/v) 26 nm, 1% (w/v) 11 nm, 2% (w/v) 5 nm silica nanoparticles, (b) mixture of 1% (w/v) 78 nm, 2.8% (w/v) 26 nm, 10% (w/v) 5 nm. Flow rate: 1 μL/min.

flow rate settings using a flow meter at the outlet of the column, and proved the accuracy and precision of flow rate including low flow rate we used in our report (Table 1). We also confirmed that the silica nanoparticles have a narrow distribution suitable for assessment of column efficiency. We measured the polydiversity index (PDI) of each silica nanoparticle by dynamic light scattering. The PDI value is an estimate of the distribution width and for a narrow distribution, a PDI of around 0.1 or lower is expected. The PDI values were 0.018 (78 nm silica), 0.022 (45 nm), 0.053 (26 nm), 0.085 (11 nm), 0.169 (5 nm). Although, PDI value of 5-nm silica nanoparticle was a little larger than 0.1, the distribution of other nanoparticles was narrow according to PDI values.

Table 1
Accuracy and precision of flow rate.

	Flow (μL/min)					
	3	2	1	0.5	0.2	0.1
Mean	2.972	1.991	0.999	0.497	0.200	0.0996
SD	0.0157	0.0083	0.0037	0.0023	0.0004	0.0003
Precision (%)	0.53	0.42	0.37	0.47	0.18	0.28
Accuracy (%)	99.08	99.56	99.93	99.30	99.81	99.59

Flow rate was measured using a flow meter according to the manufacturer's protocol. Column: Capillary EX nano Monocap Amide (500 mm × 0.2 mm i.d.); eluent: 10 mM phosphate buffer (pH 7.2) containing 20% methanol.

In SEC, for discussion of the effect of flow rate on plate height (H), Giddings' coupling theory can be simply represented by [36]

$$H = \frac{1}{(1/A)+(1/Eu)} + \frac{B}{u} + Cu. \quad (1)$$

In this equation, u is the eluent linear velocity, and A, B, C, and E are coefficients that contribute to band broadening and thus to H. The contribution of each of the terms in Eq. (1) to H are functions of (1) the coupling effect of eddy diffusion, A term (a simple flow-splitting phenomenon that is not expected to vary with linear velocity) and lateral diffusion, E term (extraparticle mass transfer in case of packed column), (2) longitudinal diffusion, B term, and (3) mass transfer, C term (solute diffuse in and out the pores and stationary-phase mass transfer effect involving basic sorption–desorption process). The curves of H *versus* u are shown in Fig. 5(a) and part of this graph was enlarged in Fig. 5(b). For sodium nitrate, the plate height is mainly determined by longitudinal molecular diffusion, which is a result of the relatively high values of B term (proportional to molecular diffusion coefficient). This causes H to increase drastically with low-velocity regions as shown in Fig. 5(b). On the other hand, the longitudinal effect (2) is generally insignificant for macromolecules, band broadening is controlled by mass transfer terms (3) or by coupling effects of eddy diffusion and lateral diffusion (1). For the mass transfer processes (C term), the magnitude of the C term is dependent on the rate of diffusion of solute in and out of the pore structure. Therefore, larger, slower-diffusing molecules increase the value of the C term more than do smaller, faster-diffusing molecules [37]. In fact, as shown in Fig. 5(a), the H *versus* u curves of silica nanoparticles were almost linear (r = 0.993–0.998) over the whole range we examined, which is different from sodium nitrate, as reported using porous silica particle columns [38]. Furthermore, the slopes of linear curves increased with an increase in the particle sizes. These results indicate that C term is a dominant plate-height term for silica nanoparticles analysis on a monolithic column.

From Fig. 5, we expected that a decrease in u should decrease H and thus increase peak resolution. In the present study, the peak resolution improved with decreasing flow rate when a mixture of different sizes of silica nanoparticles (78, 26, and 5 nm) were analyzed on a 500 mm × 0.2 mm i.d. capillary monolithic column (Fig. 6). As shown in Fig. 6, an increase in peak resolution was observed with a decrease in flow rate. The shift of peaks by the decrease in flow rate was presumably caused by an increase in permeation for nanoparticles into porous structure of silica monolith. At a flow rate of 0.1 μL/min, some aggregates were detected that were not observed at faster flow rates. A similar increase in resolution also has been reported for a mixture of proteins separated at various flow rates on a silicagel-packed column [39].

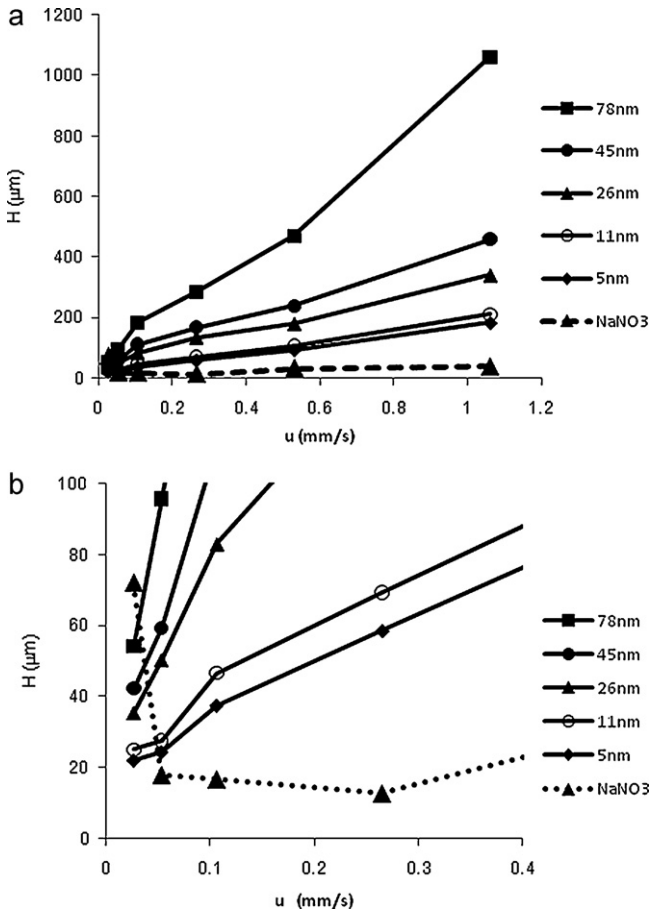

Fig. 5. (a) Plots of plate height (H) values against linear velocity of eluent (u) and (b) its low velocity region. Column: Capillary EX nano Monocap Amide (500 mm × 0.2 mm i.d.); eluent: 10 mM phosphate buffer (pH 7.2) containing 20% methanol; sample: 0.3% (w/v) 78 nm, 0.5% (w/v) 45 nm, 1% (w/v) 26 nm, 1% (w/v) 11 nm, 2% (w/v) 5 nm silica nanoparticles, and 10 μg/mL sodium nitrate.

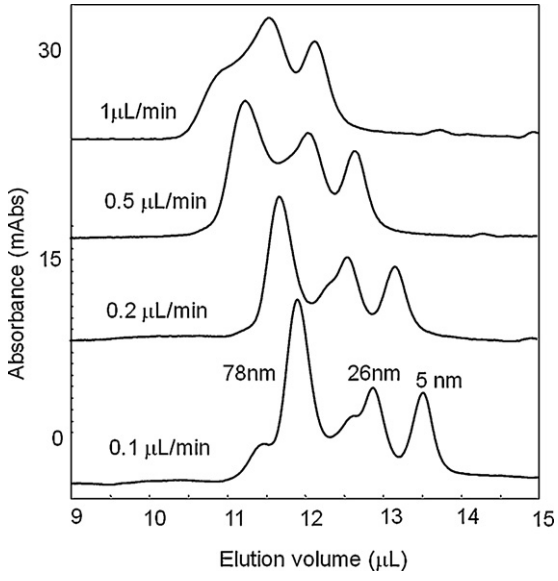

Fig. 6. Effect of flow rate on peak resolution of silica nanoparticles. Column: Capillary EX nano Monocap Amide (500 mm × 0.2 mm i.d.); eluent: 10 mM phosphate buffer (pH 7.2) containing 20% methanol; sample: mixture of 1% (w/v) 78 nm, 2.8% (w/v) 26 nm, and 10% (w/v) 5 nm silica nanoparticles; flow rate: 1, 0.5, 0.2, or 0.1 μL/min. The other conditions were the same as described in Fig. 1.

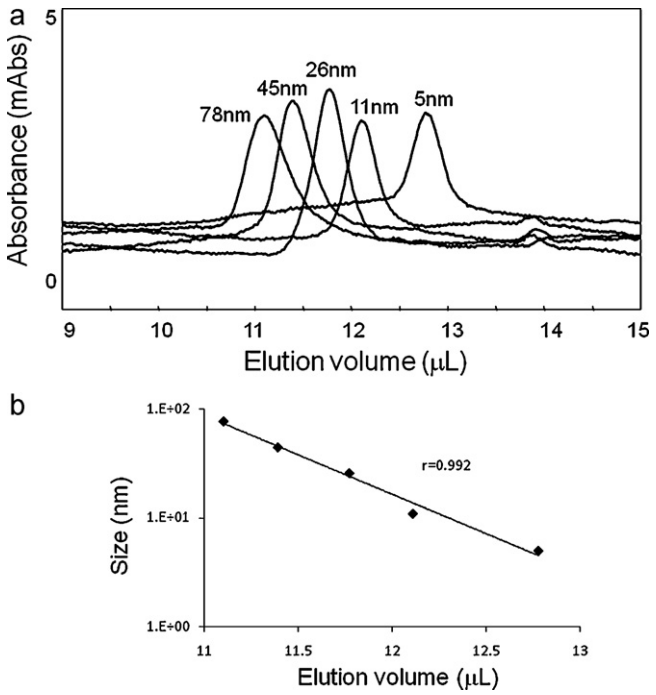

Fig. 7. (a) Particle size distribution overlay plot for five sizes of silica nanoparticles and (b) plot of the logarithm of the mass of 1 mol particles as a function of elution volume for each size of silica nanoparticles. Column: Capillary EX nano Monocap Amide (500 mm × 0.2 mm i.d.); flow rate: 0.5 μL/min; samples: solutions of 0.3% (w/v) 78 nm, 0.5% (w/v) 45 nm, 1% (w/v) 26 nm, 2% (w/v) 11 nm, and 1.5% (w/v) 5 nm silica nanoparticles. The other conditions were the same as described in Fig. 4.

3.4. Calibration curve

Fig. 7(a) shows an overlay of the particle size distribution obtained for five different samples. The nanoparticles were eluted in order of decreasing size. The logarithm of size of nanoparticles was plotted against its elution volume (Fig. 7(b)).

The plot was almost linear (r = 0.992) over a wide range of sizes including a very large size region beyond the size of mesopores (15 nm). Because SEM micrographs show the presence of very rough surfaces of the monolithic silica support in micron and submicron ranges (Fig. 8), our result indicates that not only mesopores but also these rough structures contribute to the size separation of silica nanoparticles.

We further explored the separation mechanism by drawing the molecular weight *versus* elution volume plot using dextran standards because silica nanoparticles with low molecular weight cannot be obtained. As shown in Fig. 9, the plot was linear at the high molecular weight region. Because the average hydrodynamic size of the largest dextran standard is 48 nm, this result indicates that the wide pore size distribution of the monolithic structure contributes to the selective permeation for a wide range of dextran standards and that size separation is possible beyond the range provided by the mesopores. Fig. 9 also shows that the plot curves at the low molecular weight region of below about 1000, which indicates that the permeation limit of this column exists as SEC mode.

Others also have reported that the separation of polystyrene standards according to molecular weight apparently occurred not only in the mesopores of a silica monolith (internal pore zone) but also at the outside (external pore zone) [25,40]. Ute et al. reported that when polystyrene standards were separated on a monolithic capillary column, the resulting calibration curve was linear over a wide range of masses as shown here [25]. We also examined the repeatability of the elution times using 26 and 76 nm silica nanoparticles, and relative standard deviations of the elution

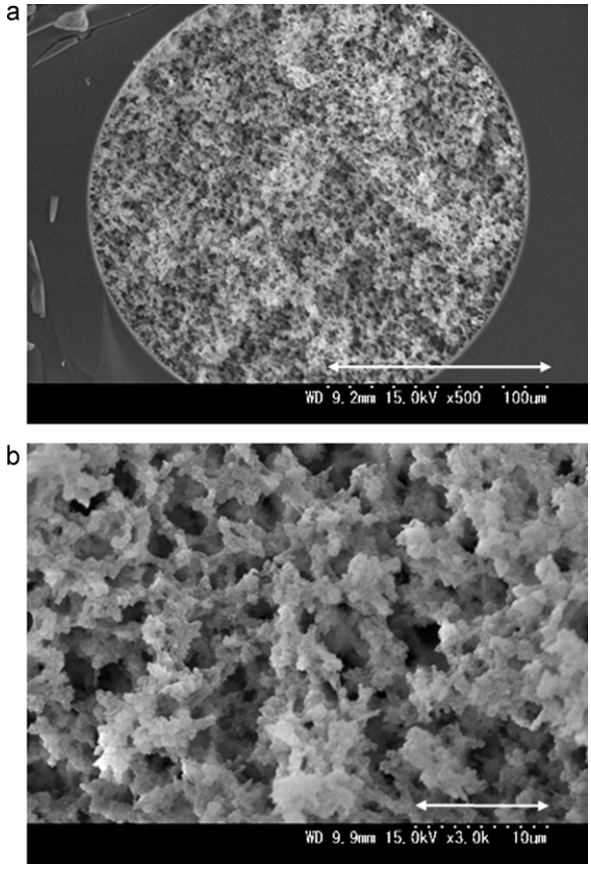

Fig. 8. Scanning electron micrographs of monolithic silica capillary columns. Scale bars corresponding to 100 μm for (a) and 10 μm for (b).

times were 0.24 and 0.15% ($n = 3$), respectively. The good linearity and repeatability of elution observed in our study indicates that this monolithic column can be used with minimal unfavorable adsorption of the solute on the column skeleton and can be used for knowledge of size and size distribution of nanoparticle samples using the calibration curve. This minimal adsorption is ascribed to alteration of the silica surface by organic functional groups. By modifying the size of mesopores or throughpores in monolithic columns, it would be possible to further clarify the separation mechanism and design columns to resolve nanoparticles with wide size ranges. Also, quantitative evaluation of particle size distribution using chromatograms remains to be solved.

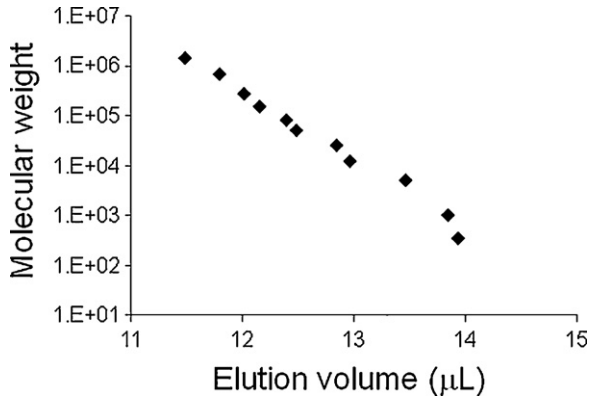

Fig. 9. Selective permeation of dextran standards. Column: Capillary EX nano Monocap Amide (500 mm × 0.2 mm i.d.); eluent: 10 mM phosphate buffer (pH 7.2) containing 20% methanol; flow rate: 1 μL/min.; sample: dextran standard; detection: UV190 nm.

4. Conclusions

In this study, we used a monolithic capillary column to develop a novel technique for the highly resolved separation of colloidally dispersed nanoparticles by their sizes. Because the column had a low backpressure, an increase in resolution could easily be achieved by elongating the column length. By optimizing the flow rate in the column, we resolved nanoparticles with only slight differences in size. The molecular weight *versus* elution volume plot curves at the low molecular weight region of below about 1000, which indicates that the permeation limit of this column exists as SEC mode. In future studies, the effect of these monolithic column structures (the sizes of mesopores and throughpores) on nanoparticle separation should be further explored to clarify the details of separation mechanism. This separation method represents a powerful means of size distribution for quality control of manufactured nanotechnology medicinal products, and this method can also be used to detect these products' impurities, including their aggregates. Therefore, this method could be used to analyze other industry-important dispersed nanomaterials, including carbon nanotubes or fullerenes.

Acknowledgements

The authors are grateful for financial support from the Research on Publicly Essential Drugs and Medical Devices Project (The Japan Health Sciences Foundation), a Health Labor Sciences Research Grant from the Ministry of Health, Labor and Welfare (MHLW), and KAKENHI (21790046) from the Ministry of Education, Culture, Sports, Science, and Technology (MEXT), Japan. The authors thank Eisai Co., Ltd. for fruitful discussion.

References

[1] M. Ferrari, Nat. Rev. Cancer 5 (2005) 161.
[2] R. Duncan, Nat. Rev. Cancer 6 (2006) 687.
[3] V.P. Torchilin, Nat. Rev. Drug Discov. 4 (2005) 145.
[4] C. Barbé, J. Bartlett, L. Kong, K. Finnie, H.Q. Lin, M. Larkin, S. Calleja, A. Bush, G. Calleja, Adv. Mater. 16 (2004) 1959.
[5] I.I. Slowing, B.G. Trewyn, S. Giri, V.S.-Y. Lin, Adv. Funct. Mater. 17 (2007) 1225.
[6] Z.Y. Zhong, K.B. Male, J.H.T. Luong, Anal. Lett. 36 (2003) 3097.
[7] K. Han, M. Yu, J. Appl. Polym. Sci. 100 (2006) 1588.
[8] R. Dastjerdi, M. Montazer, Colloids Surf. B: Biointerfaces 79 (2010) 5.
[9] C.B. Murray, D.J. Norris, M.G. Bawendi, J. Am. Chem. Soc. 115 (2002) 625.
[10] J.F. Hillyer, R.M. Albrecht, J. Pharm. Sci. 90 (2001) 1927.
[11] A. Lamprecht, Y. Bouligand, J.P. Benoit, J. Control. Release 84 (2002) 59.
[12] J. Rejman, V. Oberle, I.S. Zuhorn, D. Hoekstra, Biochem. J. 377 (2004) 159.
[13] J.J. Kirkland, J. Chromatogr. 125 (1976) 231.
[14] S.S. Huang, C.-S. Wu (Eds.), Handbook of Size Exclusion Chromatography and Related Techniques, Marcel Dekker, New York, 2004, p. 677.
[15] H. Small, J. Colloid Interface Sci. 48 (1974) 147.
[16] A. Williams, E. Varela, E. Meehan, K. Tribe, Int. J. Pharm. 242 (2002) 295.
[17] J.C. Giddings, Science 260 (1993) 1456.
[18] J.C. Giddings, Anal. Chem. 67 (1995) 592A.
[19] M.H. Moon, I. Park, Y. Kim, J. Chromatogr. A 813 (1998) 91.
[20] C.A. Silebi, J.G. Dosramos, J. Colloid. Interface Sci. 130 (1989) 14.
[21] B.B. VanOrman, G.L. McIntire, J. Microcolumn Sep. 1 (1989) 289.
[22] H. Ahmadzadeh, R. Dua, A.D. Presley, E.A. Arriaga, J. Chromatogr. A 1064 (2005) 107.
[23] Y.H. Rezenom, A.D. Wellman, L. Tilstra, C.D. Medley, S.D. Gilman, Analyst 132 (2007) 1215.
[24] C. Grabielle-Madelmont, S. Lesieur, M. Ollivon, J. Biochem. Biophys. Methods 56 (2003) 189.
[25] K. Ute, S. Yoshida, T. Kitayama, T. bamba, K. Harada, E. Fukusaki, A. Kobayashi, N. Ishizuka, H. Minakuchi, K. Nakanishi, Polym. J. 38 (2006) 1194.
[26] H. Minakuchi, K. Nakanishi, N. Soga, N. Ishizuka, N. Tanaka, Anal. Chem. 68 (1996) 3498.
[27] N. Tanaka, H. Kobayashi, K. Nakanishi, H. Minakuchi, N. Ishizuka, Anal. Chem. 73 (2001) 420A.
[28] K.K. Unger, Porous Silica; Journal of Chromatography Library, vol. 16, Elsevier, Amsterdam, 1979.

[29] K. Miyamoto, T. Hara, H. Kobayashi, H. Morisaka, D. Tokuda, K. Horie, K. Koduki, S. Makino, O. Núñez, C. Yang, T. Kawabe, T. Ikegami, H. Takubo, Y. Ishi hama, N. Tanaka, Anal. Chem. 80 (2008) 8741.
[30] G. Guiochon, J. Chromatogr. A 1168 (2007) 101.
[31] A. Zattoni, E.L. Piccolomini, G. Torsi, P. Reschiglian, Anal. Chem. 75 (2003) 6469.
[32] Z. Aspanut, T. Yamada, L.W. Lim, T. Takeuchi, Anal. Bioanal. Chem. 391 (2008) 353.
[33] T. Takeuchi, Siswoyo, Z. Aspanut, L.W. Lim, Anal. Sci. 25 (2009) 301.
[34] J. Depasse, A. Watillon, J. Colloid Interface Sci. 33 (1970) 430.
[35] F. Gritti, C.A. Sanchez, T. Farkas, G. Guichon, J. Chromatogr. A 1217 (2010) 3000.
[36] J.C. Giddings, Dynamics of Chromatography: Principles and Theory, Marcel Dekker, New York, 1965, p. 62.
[37] A. Striegel, W.W. Yau, J.J. Kirkland, D.D. Bly, Modern Size-Exclusion Liquid Chromatography: Practice of Gel Permeation and Gel Filtration Chromatography, John Wiley and Sons, Inc., New Jersey, 2009, p. 55.
[38] G. Stegeman, J.C. Kraak, H. Poppe, J. Chromatogr. 550 (1991) 721.
[39] H. Engelhardt, U.M. Schon, Chromatographia 22 (1986) 388.
[40] M. Al-Bokari, D. Cherrak, G. Guiochon, J. Chromatogr. A 975 (2002) 275.